Structural Chemistry
https://doi.org/10.1007/s11224-024-02366-6

RESEARCH

Nature of the chemical bonding and electronic structure of dicoordinated copper(I) complexes of alkenes, alkynes, and NHC ligands: a DFT overview

Nadjet Aimene[1] · Abdallah Zaiter[1,2] · Hacene Nemdili[1] · Bachir Zouchoune[1,2]

Received: 21 May 2024 / Accepted: 6 August 2024

Abstract
A DFT (density functional theory) investigation using the generalized gradient approximation BP86 and the hybrid B3LYP functionals and TZP basis set is dealing with the bonding, the electronic structure and the interaction types occurred within the XCuL' and $(LCuL')^+$ (X = Cl, CH_3, CN, CF_3, L = CO, NH_3, PH_3, and L' = C_2H_2, C_2H_4, C_4H_6, C_6H_6, and NHC) complexes. The optimized structures and energy decomposition analysis of XCuL' and $(LCuL')^+$ complexes were employed to provide a relationship between the bond lengths, the X-Cu-L' and L-Cu-L' bond angles, the Wiberg indices, the Mayer bond orders, interaction energies, and the Cu-L' bonding character. The energy decomposition analysis indicates that the interactions occurred for various L' ligands are more electrostatically than covalently bonded to the Cu(I) center formally of +I oxidation state. The different contributions stemming from electrostatic and orbital interactions are significant, in relationship with the ionic and covalent characters, respectively. The contribution from σ-donation to the bonding energy was found more important for the NHC ligand than the alkene and alkynes ones. However, the contribution from π-back-donation was found to be comparable for all complexes. The σ-bonding contributes more than 50% into the total orbital interaction overtaking those of π type, in accordance with the population of the copper 4s orbital, particularly in the presence of C_6H_6 and NHC ligands. The interactions in all complexes exhibit comparable deformation densities and NOCV orbital shapes. Besides, it has been shown that the ΔE_{prep} contributes weakly in the deformation of the interacting fragments as well as the BSSE correction which impacts weakly or negligibly the interactions between the fragments composing different XCuL' and $(LCuL')^+$ complexes.

Keywords Coordination chemistry · Electron transfers · Energy decomposition analysis · Deformation energy · BSSE contribution

Introduction

The Cu(I), Ag(I) and Au(I) as transition metals d^{10} cations adopt various coordination modes with different ligands corresponding to outstanding linear, trigonal planar and tetrahedral molecular structures [1–4] with probable applications as phosphors in organic light emitting diodes (OLEDs) for Cu(I) complexes [5, 6].

✉ Nadjet Aimene
aimenenadjet@gmail.com

1 Unité de Recherche de Chimie de L'environnement Et Moléculaire Structurale, Université Constantine 1 (Mentouri), Constantine 25000, Algeria

2 Laboratoire de Chimie Appliquée et Technologie des Matériaux, Université Larbi Ben M'Hidi-Oum El Bouaghi, Oum El Bouaghi 04000, Algeria

The linear two-coordinated Cu(I) complexes targeted in this investigation have been experimentally explored and theoretically analyzed [7, 8], particularly, those of monodendate nitrogen ligands which are represented. These types of complexes are rarely characterized due to their relative instability due to electronic factors [9–13], but the sterically hindered ligands enhance their stability [9].

However, the linear Cu(I) carbene complexes have been extensively investigated owing of their interesting photophysical characteristics resulting from ligand-to-ligand charge transfer [14–16], where several of them have been used as emitters [17, 18] exhibiting interesting luminescence properties [19–21]. Indeed, linear di-coordinate copper complexes of cyclic(alkyl)(amino)-carbenes (CAAC) CuX (X = Cl, Br, I) display photoluminescence as the first species highly luminescent [22] and showing remarkable

Published online: 14 August 2024

photophysical properties when compared to their analogous N-heterocyclic carbene complexes [23].

The linear Cu(I) and Ag(I) alkene or alkyne compounds are scarcely characterized by XR-diffraction [24, 25], despite that this class of compounds is the first reported among organometallic ones, contrary to their homologous of Au(I) which are more isolated and characterized [26–31].

The XCuL' and $(LCuL')^+$ (L = CO, PH_3, NH_3, L' = NHC, C_2H_2, C_2H_4, C_4H_6, C_6H_6, and X^- = Cl, CH_3, and CN) complexes of 14-MVE (metal valence electrons) count are investigated throughout this theoretical study and are compared to their homologous LML' compounds known to adopt a linear structure with L-M-L' angle of about 180° [32, 33].

Within this work, the molecular and electronic structures were investigated for each L' ligand in relationship with its bonding towards the XCu or $(LCu)^+$ metallic moiety based on the identification of different interactions, where X^- and L as terminal ligands are isoelectronic units, but with different properties; it is what we ought to elucidate.

Furthermore, in order to assess the σ-donation and π-backdonation of various used ligands, the interactions have been evaluated between XCu and L' fragments on one hand and between LCu^+ and L' on other hand using the energy decomposition analysis (EDA) [34–36] combined with natural orbital for chemical valence (EDA-NOCV) [37–41] analysis taking into account the impact of X or L ligand composing the XCu or LCu^+ fragments of 12-MVE count. The EDA provides a connection between the physical rules of quantum mechanics and a conceptually simple explanation of nature chemical bonding. Besides, the EDA-NOCV method connects the frontier orbital theory of Fukui [42] and the orbital symmetry rules of Wood-Ward and Hoffmann [43] resulting from DFT calculations.

Thus, we present a detailed analysis of the coordination between acetylene as alkyne, ethylene, butadiene and benzene as alkene or NHC and the XCu' or $(LCu)^+$ metallic fragment, where a complete rationalization of bonding is provided of this kind of complexes with respect to X, L, and L' ligands in order to establish the similarities and discrepancies of the occurred interactions.

Theoretical methods

The density functional theory (DFT) calculations have been performed to optimize all molecular structures at the BP86 [44–47] and B3LYP [48, 49] computational levels. The electron correlation was treated within the local density approximation (LDA) in the Vosko–Wilk–Nusair parametrization [50]. The triple-ξ polarization basis set for all atoms and the frozen core approximation for BP86 functional using the ADF2022.01 program [51] developed by Baerends and co-workers [52–56]. Frequency calculations have been performed on the optimized structures to authenticate that the obtained structures correspond to energetic minima [57, 58]. The natural population-based (NPA) and Wiberg bond indices [54, 59] were obtained from calculations implemented in the NBO 7.0 program [60, 61]. The EDA-NOCV [37–41] method results from the combination between natural orbitals for chemical valence (NOCV) [37–41] and energy decomposition analysis (EDA) [34–36] was applied to decompose the deformation density correlated to the bond formation into various components of the chemical bonding. The EDA-NOCV scheme divides the orbital interactions between the interacting fragments into pairwise contributions of the most relevant molecular orbitals. Furthermore, The Mayer bond orders (MBO) [62–64] have been calculated which can be seen as an expansion of the Wiberg bond indices implemented in the ADF2022.01 program [51].

Results and discussions

Free ligands

The C_2H_2, C_2H_4, C_4H_6 and C_6H_6, and NHC as free ligands were optimized to get information about their structures (Fig. 1) and their π-electrons localization. Indeed, the C_2H_2 (acetylene) as alkyne molecule displays a C–C bond distance of 1.231 Å and a linear C–C-H angle of 180° matching well with a triple bond as known in the literature [64]. However, C–C bond distances in the plane C_2H_4 (ethylene) molecule and C_4H_6 (butadiene) as alkene are of 1.332 and 1.343 Å corresponding to a double bond describing a localized scheme comparable to the experimental values and reproducing theoretical findings [66–68], but in C_6H_6 (benzene) aromatic ring, the average C–C bond distance is of 1.398 Å matching well with a delocalized scheme and corresponds to 1.5 bond order as obtained in previous works [69–77].

XCUL' and $(LCuL')^+$ optimized structures

The optimized structures of the XCuL' and $(LCuL')^+$ compounds are shown in Figs. 2 and 3, and their relevant geometrical parameters obtained by means of BP86 and B3LYP are gathered in Tables S1 and S2, and compared to those experimentally observed when they are available. Firstly, we discuss the structures of XCu(C_2H_2), XCu(C_2H_4), XCu(C_4H_6), XCu(C_6H_6), and XCu(NHC) displaying large HOMO–LUMO gaps to get information about the change of the Cu-C(1) and Cu-C(2) bond distances related to the coordination mode of the XCu metallic fragment induced by the introduction of L' ligand. Besides, the C(1)-C(2) bond distances calculated within the free L' ligands are compared to their corresponding ones in XCuL' compounds. In recent

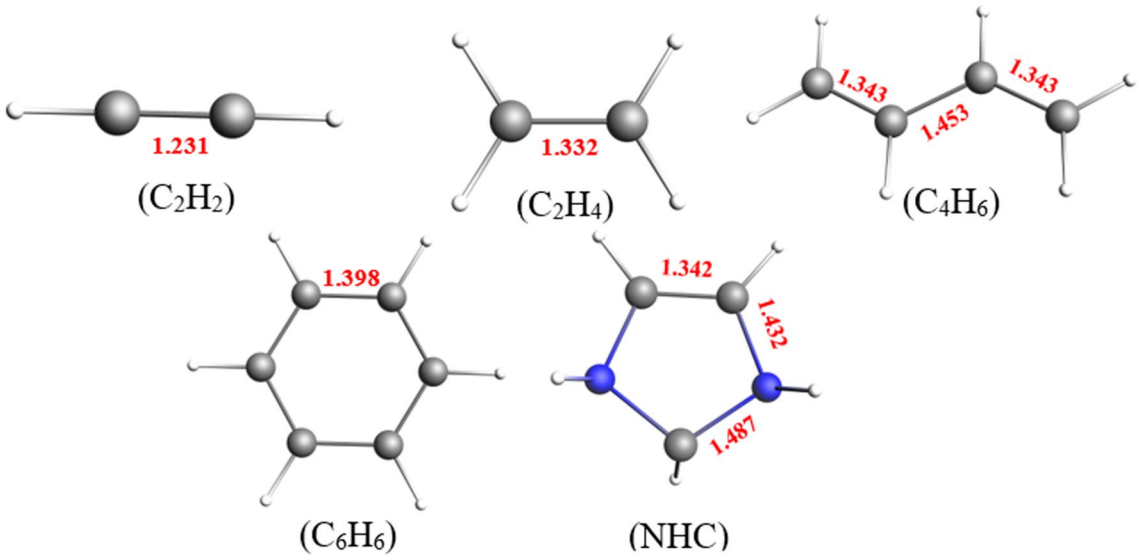

Fig. 1 BP86-optimized structures of free ligands with C–C and C-N bond distances in Å

work, it has been shown that the X-Cu-L' angle encountered in XCu(CAAC)] (X = Cl, Br, I, and CAAC = cyclic(alkyl)(amino)carbene) compound [19, 77] showed a linearity of L-Cu-L bond angle comparable to those computed for CH_3Cu(NHC) and CNCu(NHC) varying from 161° to 180°. One can remark that for each XCu fragment the Cu-C(L') bond distance varies in function of the variation of the X ligand. The shortest Cu-C(L') bond distance of 1.891 Å corresponds to the Cu-C in CH_3Cu(NHC) comparable to those found in previous works [24, 78], while the longest one corresponds to the Cu-C in CNCu(C_6H_6) of 2.175 Å as given in Table S1, comparable to those experimentally reported in the literature [79] relative to Cl-Cu bond distance of 2.099 Å, which is similar to those computed for ClCuL' compounds ranging from 2.089 to 2.097 Å. It is interesting to mention that for each L', the shortest Cu-C(L') is obtained in ClCuL' compounds followed respectively by those in CH_3CuL' and CNCuL' ones, giving rise to η^2-coordination mode in the presence of C_2H_2, C_2H_4, C_4H_6, and C_6H_6. Considering the results gathered in Table S1, there is a perfect correlation between the Wiberg bond indices (WBI), Mayer bond orders (MBO), and the bond distances shortening or lengthening of the Cu-L' bond distances. Indeed, the WBI and MBO values tend to become larger when the bond distances become short as well illustrated in Table S1. So, the shortest Cu-C(L') bond distance is obtained in the case of the NHC compounds corresponding to WBI of 0.51, 0.46, 0.43, and 0.45 and MBO of 0.89, 0.85, 0.83 and 0.84 when it is attached to ClCu, CH_3Cu, CF_3, and CNCu metallic fragments, respectively. However, the WBI values for Cu-C(C_6H_6) bond fall to 0.29 (0.14 + 0.15), 0.28 (0.14 + 0.14), 0.32 (0.16 + 0.16), and 0.36 (0.18 + 0.18) in the presence of CN^-, CF_3^-, CH_3^-, and Cl^- anions, respectively, corresponding to the longest Cu-C bond lengths. Besides, Mayer bond orders listed in Tables S1 and S2 show large values compared to those of WBI ones, putting emphasis on a σ-dative L → Cu bond, i.e., the interaction are interpreted as a dative or donor–acceptor bond [80].

A higher positive charge at the Cu(I) cation signifying a considerable charge donation and vice versa in all XCu(NHC) complexes. The findings relative to the electronic configuration show obviously that there is a correlation between the charge of the Cu(I) cation and the 4s and 3d orbitals' populations (Table S1). The most populated 4s orbital is encountered in the XCu(NHC) compounds regardless the X ligand indicating considerable σ-donation from the HOMO orbital of the NHC ligand towards the antibonding vacant XCu orbital mostly of 4s character. However, the 3d orbital is weakly depopulated in agreement with a very weak π-backdonation into the vacant π*C-N antibonding orbital of the NHC ligand as clearly given in Table S1.

It is interesting to mention that the C = C bond length modifications when it is coordinated to different XCu fragments undertaking somewhat elongations in accordance with the L' ligand. Indeed, the major C = C elongations are obtained in the cases of C_6H_6 and C_4H_6 of 1.424 and 1.382 Å compared to those of free ligands of 1.398 Å and 1.343 Å, respectively. Besides, the C–C-H linear angle of the free C_2H_2 ligand (Fig. 1) undertakes deformation in various XCu(C_2H_2) complexes and becomes bent one by 16° as elucidated in Fig. 2.

For each XCuL' compound, the C = C elongations obey the following tendency in accordance with the L' ligand: $C_6H_6 > C_2H_2 \approx C_2H_4 > C_4H_6$. Similarly, the

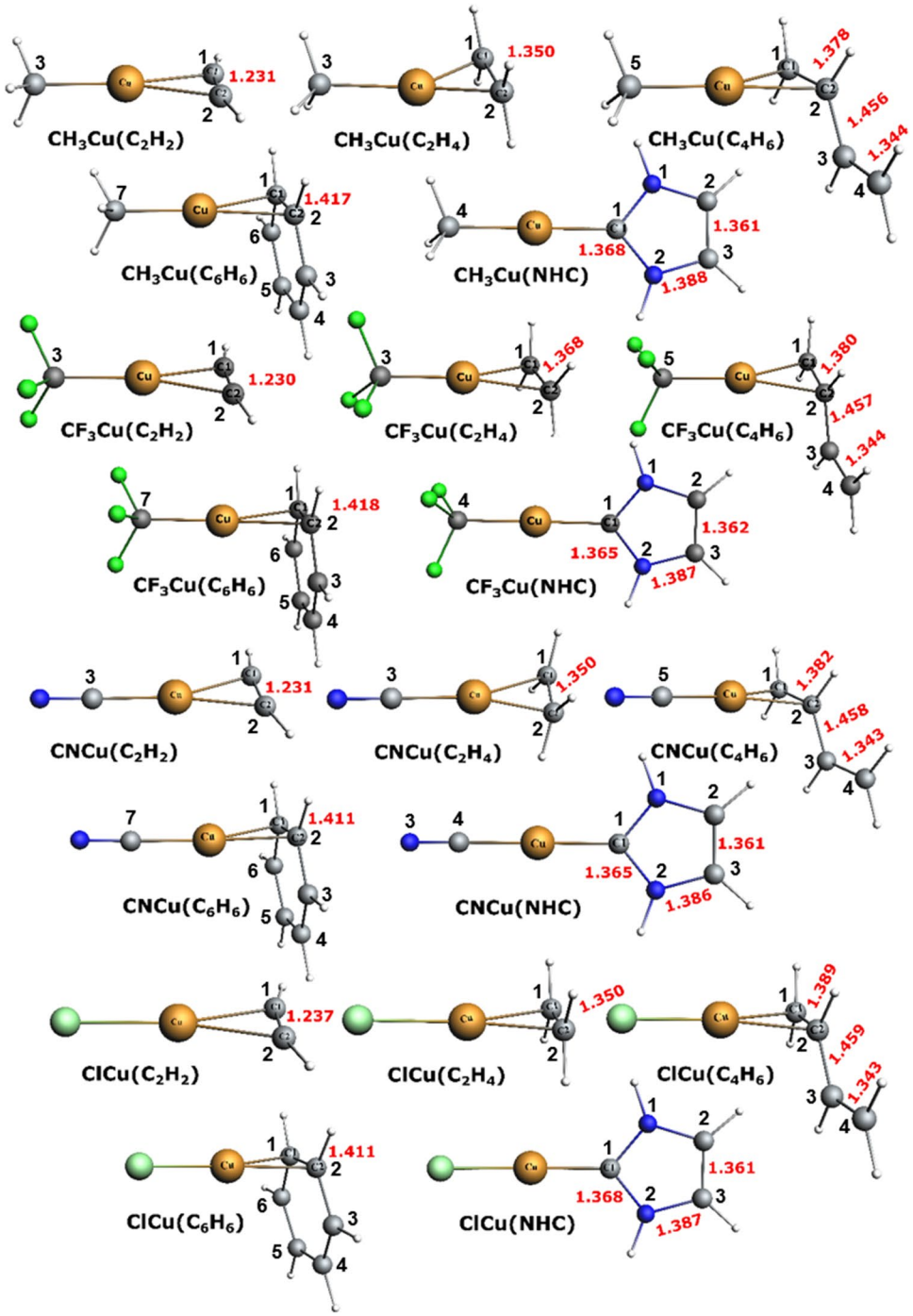

Fig. 2 The lowest BP86-optimized XCuL' structures of singlet state and their atom numbering adopted throughout the paper. The C–C and C-N bond distances are given in Å

$(LCuL')^+$ compounds exhibit comparable tendencies than those observed for XCuL', but with somewhat differences concerning the Cu-C(L') and C(1)-C(2) bond lengths.

In $(LCuL')^+$, the Cu-C(L') bond distances are slightly longer by about 0.05 Å than those obtained in their analogous of XCuL' as gathered in Table S2. Moreover, the Cu-C bond distances in $(COCuL')^+$ are weakly longer than those encountered in $(PH_3CuL')^+$. The C = C bond distances within these compounds undergo elongation as sketched in Fig. 3. All $(LCuL')^+$ structures display very large HOMO–LUMO gaps ranging from 2.96 to 5.18 eV (BP86) or 4.36 to 6.15 eV (B3LYP) predicting stable compounds.

Furthermore, L-Cu-L' angles in all $(LCuL')^+$ structures are linear or deviate slightly from the linearity with regard to their values ranging from 161 to 180° as described for related complexes [81].

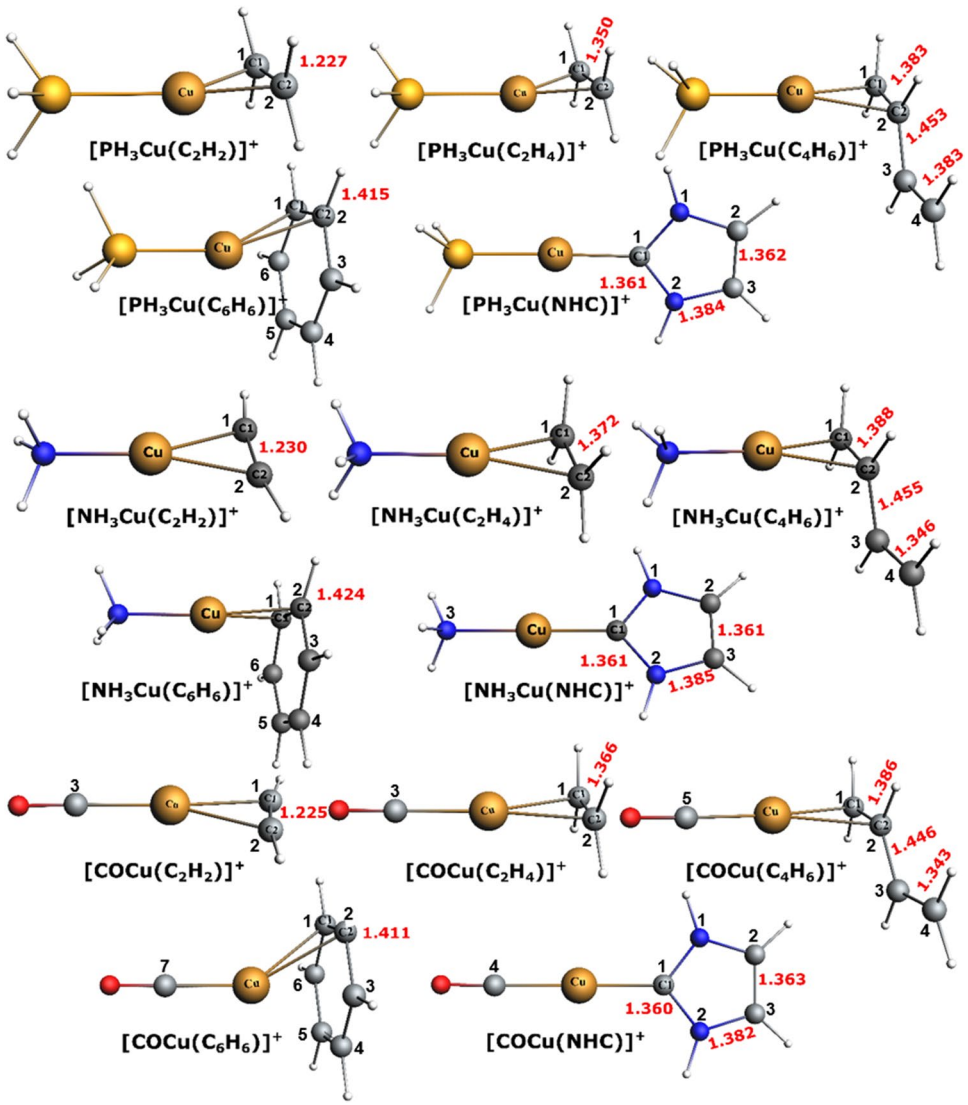

Fig. 3 The lowest BP86-optimized $(LCuL')^+$ structures of singlet state and their atom numbering adopted throughout the paper. The C–C and C-N bond distances are given in Å

Energy decomposition analysis

The Morokuma–Ziegler energy decomposition analysis (EDA) [34–36] is a powerful method for a quantitative explanation of chemical bonding and largely used recently [82–93]. Within this work, the EDA is applied to describe the nature of the interactions between XCu and L' on one hand (Table 1) and between $(LCu)^+$ and L' on other hand (Table 2). The total bonding energy ΔE_{Bond} is considered as the combination between the preparation energy ΔE_{prep} (or strain energy, deformation energy) and the interaction energy ΔE_{int} as summarized in Tables 1 and 2. The preparation energy is the quantity of energy that is necessitated to deform XCu and L' on one hand and LCu^+ and L' on other hand from their equilibrium structures to the geometries they have in the XCuL' and $[LCuL']^+$ complexes (it is identified as the difference between the isolated fragments and the states found in the final complex). Thus, the preparation energy (ΔE_{prep}) is the difference between ΔE_{int} and ΔE_{Bond}: $\Delta E_{prep} = \Delta E_{Bond} - \Delta E_{int}$. Furthermore, for a molecule AB composed of A and B molecular fragments, the preparation energy (ΔE_{prep}) can be expressed as follows: $\Delta E_{prep} = [E(A)_{AB} - E(A)] + [E(B)_{AB} - E(B)]$, where $E(A)_{AB}$ and $E(B)_{AB}$ are respectively the energies of A and B fragments calculated in the optimized AB molecule, whereas E(A) and E(B) are respectively the energies of A and B in their optimized states corresponding to the isolated structures. The most important conclusion that arises from the calculations of the preparation energy ΔE_{prep} is that its contribution is weak in the ranges 0.5–4.4 and 0.1–2.8 kcal/mol for XCuL' and $[LCuL']^+$ complexes, respectively, as gathered in Tables 1 and 2. The most important value of ΔE_{prep} of 4.4 kcal/mol corresponds to the deformation of the C_2H_2 ligand which losses its linearity through the bending of C–C-H angle shifting from 180° (free ligand) to 163° in $ClCu(C_2H_2$. However, it has been observed that C_2H_4, C_4H_6,

Table 1 The ΔE_{int}, ΔE_{prep}, and ΔE^{CP} (counterpoise) energies of BP86 functional arising from the interaction between XCu (X = CH_3, CF_3, CN, Cl) and L' (L' = C_2H_2, C_2H_4, C_4H_6, C_6H_6, NHC) fragments in kcal/mol. Contribution (%) of each ΔE_{elstat} and ΔE_{orb} component into the total attractive energy ($\Delta E_{elstat} + \Delta E_{orb}$) is given in parentheses and the electronic populations of σ and π orbitals derived from the natural population analysis are given between square brackets

	ΔE_{int}	ΔE_{prep}	ΔE^{CP}	ΔE_{Pauli}	ΔE_{elstat}	ΔE_{orb}	$\Delta E(\sigma)$	$\Delta E(\pi)$	$\Delta E(rest)$
$CH_3Cu(C_2H_2)$	−28.1	3 9	−27.6	106.8	−83.9 (62%)	−51.0 (38%)	−26.5 (52%) [1.70]^a	−19.5 (39%) [0.19]^b	−4 (9%)
$CH_3Cu(C_2H_4)$	−26.7	2.5	−27.2	100.7	−79.3 (62%)	−48.1 (38%)	−27.4 (57%) [1.69]^a	−18.3 (38%) [0.19]^b	−2.4 (5%)
$CH_3Cu(C_4H_6)$	−25.8	2.5	−25.3	99.7	−77.2 (62%)	−48.3 (38%)	−26.1 (54%) [1.81]^a	−19.8 (41%) [0.16]^b	−2.4 (5%)
$CH_3Cu(C_6H_6)$	−18.7	1.6	−18.1	82.8	−61.4 (60%)	−40.1 (40%)	−31.5(79%) [1.87]^a	−5.4 (13.4%) [0.03]^b	−3.2 (8%)
$CH_3Cu(NHC)$	−48.6	1.2	−48.3	123.2	−132.1 (77%)	−39.7 (23%)	−23.9 (60%) [1.50]^a	−14.3 (36%) [0.09]^b	−1.5 (4%)
$CF_3Cu(C_2H_2)$	−31.9	3.5	−31.2	98.6	−80.8 (62%)	−49.7 (38%)	−25.4 (52%) [1.68]^a	−21.5 (43%) [0.15]^b	−2.5 (5%)
$CF_3Cu(C_2H_4)$	−31.1	2.5	−30.4	91.4	−75.3 (62%)	−47.1 (38%)	−23.1 (49%) [1.66]^a	−21.6 (46%) [0.15]^b	−2.4 (5%)
$CF_3Cu(C_4H_6)$	−30.8	2.8	−30.0	88.9	−72.4 (61%)	−47.4 (38%)	−22.2 (47%) [1.79]^a	−21.7 (46%) [0.12]^b	−3.5 (7%)
$CF_3Cu(C_6H_6)$	−25.1	1.8	−24.2	77..8	−60.2 (59%)	−42.7 (41%)	−20.6 (48%) [1.83]^a	−17.8 (42%) [0.08]^b	−4.3 (10%)
$CF_3Cu(NHC)$	−58.7	1.8	−57.7	118.3	−136.0 (77%)	−41.0 (23%)	−26.5 (65%) [1.49]^a	−12.3 (30%) [0.07]^b	−2.2 (5%)
$CNCu(C_2H_2)$	−37.8	3.2	−37.1	91.3	−78.4 (61%)	−50.7 (39%)	−27.4 (54%) [1.67]^a	−20.8 (41%) [0.17]^b	2.5 (5%)
$CNCu(C_2H_4)$	−37.0	1.2	−36.3	84.7	−73.6 (60%)	−48.2 (40%)	−25.8 (54%) [1.69]^a	−21.3 (44%) [0.16]^b	−1.1 (2%)
$CNCu(C_4H_6)$	−36.7	2.3	−35.9	83.2	−70.9 (59%)	−48.9 (41%)	−24.5 (50%) [1.78]^a	−22.5 (46%) [0.13]^b	−1.9 (4%)
$CNCu(C_6H_6)$	−30.3	1.4	−29.4	71.0	−57.2 (57%)	−44.1 (43%)	−33.6 (76%) [1.83]^a	−7.2 (16%) [0.09]^b	−3.3 (8%)
CNCu(NHC)	−64.6	0.7	−63.7	111.3	−135.5 (77%)	−40.3 (23%)	−25.5 (63%) [1.49]^a	−12.9 (32%) [0.07]^b	−1.9 (5%)
$ClCu(C_2H_2)$	−42.8	4.4	−42.2	101.4	−86.6 (60%)	−57.6 (40%)	−31.7 (55%) [1.66]^a	−23.4 (41%)[0.22]^b	−2.5 (4.3%)
$ClCu(C_2H_4)$	−41.7	0.5	−41.0	95.2	−82.5 (60%)	−54.4 (40%)	−30.6 (56%) [1.63]^a	−22.5 (41%) [0.22]^b	−1.3 (3%)
$ClCu(C_4H_6)$	−40.6	3.0	−39.8	92.2	−78.7 (59%)	−54.1 (41%)	−29.2 (54%)[1.77]^a	−22.1 (41%) [0.17]^b	−2.8 (5%)
$ClCu(C_6H_6)$	−32.5	2.1	−31.7	79.3	−63.9 (57%)	−47.9 (43%)	−38.5 (80%) [1.93]^a	−5.8 (12%) [0.06]^b	−3.6 (8%)
ClCu(NHC)	−65.7	0.5	−64.8	118.8	−141.9 (77%)	−42.6 (23%)	−25.7 (60%) [1.48]^a	−15.5 (36%) [0.10]^b	−1.4 (4%)

C_6H_6, and NHC ligands are less distorted, particularly the NHC fragment composing the LCu(NHC) complex which it does not undergo any deformation behaving as rigid molecule as evidenced in Table 1. The LCu^+ and L' in $(LCuL')^+$ are relatively less sensitive to the deformation, in relationship with their ΔE_{prep} values gathered in Table 2 compared to those obtained for XCuL' compounds.

Table 1 gathers the results of the energy decomposition analysis (EDA) arising from the interactions between XCu and L'. The EDA scheme decomposes the bonding interaction energy ΔE_{int} into three terms of energies: the classical electrostatic interactions ΔE_{elstat} and the orbital term ΔE_{orb} as attractive terms and the ΔE_{Pauli} repulsion exchange term are comparable. Thus, the Cu-L' interaction energies ΔE_{int} collected in Table 1 have different negative amounts, but display the same trend recorded for all XCuL' compounds. The ΔE_{int} shows that for each L' ligand, the strongest interactions are calculated for ClCu fragment corresponding to the highest absolute value and obeying the decreasing order ClCu > CNCu > CF_3Cu > CH_3Cu. Really, Table 1 and the plots of Fig. 4 demonstrate that the interaction energies ΔE_{int} of the ClCuL' complexes are about 5, 10, and 15 kcal/mol lower than the values of their corresponding obtained for CNCuL', CF_3CuL', and CH_3CuL' complexes, respectively, except for the NHC ligand whose values are comparable for the ClCu and CNCu fragments, as clearly illustrated. For each XCu fragment, the most significant interactions are found for NHC ligand and the weakest ones are encountered for C_6H_6, while the C_2H_2, C_2H_4, and C_2H_6 ligands exhibit comparable energies as well summarized in Table 1.

In each case of the XCuL' compounds, the largest contribution into the ΔE_{int} value stems from the ΔE_{Pauli} repulsive term, but it is overbalanced by the total attractive contribution ($\Delta E_{elstat} + \Delta E_{orb}$) giving rise to stabilizing interactions as highlighted by the negative values of ΔE_{int}. The proportion of the ΔE_{elstat} electrostatic attractive energy is higher than that of the ΔE_{orb} one which comes from the orbital relaxation and orbital mixing between the interacting fragments. The lowest ΔE_{elstat} contribution is observed for all C_6H_6 compounds which ranges from 44% (CNCu(C_6H_6) to 60% ($CH_3Cu(C_6H_6)$; however, it substantially enhances to 77% for the NHC ligand in all XCuL' compounds. The main part of the repulsive term ΔE_{Pauli} as an exchange repulsion stems from the interaction between occupied orbitals of the XCu fragment and the occupied π orbitals of the L' ligand in the cases of C_2H_2, C_2H_4, C_2H_6, and C_6H_6 and the occupied σ-type orbital of NHC. The results given in Table 1 show clearly that NHC is the strongest σ-donor, but the weakest π-acceptor as reported in previous works [77]. It is interesting to mention the comparable behavior of C_2H_2, C_2H_4, and C_4H_6 ligands regarding ΔE_{int} and its components, while C_6H_6 behaves differently due probably to the π-electrons

Table 2 The ΔE_{int}, ΔE_{prep}, and ΔE^{CP} (counterpoise) energies of BP86 functional arising from the interaction between $(LCu)^+$ (L = PH_3, NH_3, CO) and L' (L' = C_2H_2, C_2H_4, C_4H_6, C_6H_6, NHC) fragments are given in kcal/mol. Contribution (%) of each ΔE_{elstat} and ΔE_{orb} component into the total attractive energy ($\Delta E_{elstat} + \Delta E_{orb}$) is given in parentheses and the electronic populations of σ and π orbitals derived from the natural population analysis are given between square brackets

	ΔE_{int}	ΔE_{prep}	ΔE^{CP}	ΔE_{Pauli}	ΔE_{elstat}	ΔE_{orb}	$\Delta E(\sigma)$	$\Delta E(\pi)$	$\Delta E(rest)$
$[PH_3Cu(C_2H_2)]^+$	−43.9	2.5	−42.7	74.4	−69.3 (59%)	−49.0 (41%)	−25.7 (53%) [1.62][a]	−21.2 (43%) [0.09][b]	−2.1 (4%)
$[PH_3Cu(C_2H_4)]^+$	−44.3	1.4	−43.2	68.1	−64.3 (57%)	−48.1 (43%)	−27.7 (57.6%) [1.59][a]	−18.1 (37.7%) [0.09][b]	−2.3 (5%)
$[PH_3Cu(C_4H_6)]^+$	−48.3	2.8	−47.0	68.7	−63.8 (55%)	−53.2 (45%)	−31.7 (60%) [1.71][a]	−18.3 (34%) [0.07][b]	−3.2 (6%)
$[PH_3Cu(C_6H_6)]^+$	−45.8	0.9	−44.0	70.4	−57.4 (50%)	−58.8 (50%)	−33.4 (56.8%) [1.70][a]	−16.2 (28%) [0.04][b]	−9.2 (16%)
$[PH_3Cu(NHC)]^+$	−87.1	1.4	−85.2	104.8	−141.8 (74%)	−50.1 (26%)	−32.4 (65%) [1.43][a]	−14.3 (28%) [0.04][b]	−3.4 (7%)
$[NH_3Cu(C_2H_2)]^+$	−50.1	2.8	−48.9	80.5	−76.4 (58.5%)	−54.2 (41.5%)	−25.5 (47%) [1.60][a]	−25.8 (48%) [0.12][b]	−2.9 (5%)
$[NH_3Cu(C_2H_4)]^+$	−45.5	0.1	−44.2	72.2	−66.6 (57%)	−51.1 (43%)	−30.6 (60%) [1.60][a]	−17.6 (35%) [0.10][b]	−2.8 (5%)
$[NH_3Cu(C_4H_6)]^+$	−53.7	2.8	−52.3	73.7	−70.2 (55%)	−57.3 (45%)	−33.7 (59%) [1.70][a]	−18.7 (33%) [0.09][b]	−1.8 (3%)
$[NH_3Cu(C_6H_6)]^+$	−49.1	1.4	−47.5	66.8	−59.7 (52%)	−56.2 (48%)	−34.6 (62%) [1.79][a]	−13.7 (24%) [0.06][b]	−0.8 (4%)
$[NH_3Cu(NHC)]^+$	−92.0	0.9	−90.6	109.6	−150.5 (75%)	−51.2 (25%)	−32.8 (64%) [1.43][a]	−15.1 (30%) [0.05][b]	−3.3 (6%)
$[COCu(C_2H_2)]^+$	−51.1	1.8	−49.7	58.4	−59.98 (55%)	−49.5 (45%)	−30.5 (62%) [1.56][a]	−16.5 (33%) [0.07][b]	−2.5 (5%)
$[COCu(C_2H_4)]^+$	−50.1	0.1	−48.6	64.7	−64.9 (57%)	−49.9 (43%)	−30.4 (61%) [1.59][a]	−17.3 (34.5%) [0.07][b]	−2.2 (4.5%)
$[COCu(C_4H_6)]^+$	−57.8	2.8	−56.2	57.2	−57.8 (50%)	−57.2 (50%)	−38.3 (67%) [1.65][a]	−15.1 (26%) [0.06][b]	−3.8 (7%)
$[COCu(C_6H_6)]^+$	−58.9	0.7	−56.6	68.6	−57.1 (45%)	−70.4 (55%)	−38.0 (54%) [1.64][a]	−20 (28.4%) [0.04][b]	−12.4(18%)
$[COCu(NHC)]^+$	−99.9	0.9	−98.5	99.3	−145.3 (73%)	−53.9 (27%)	−33.6 (62%) [1.42][a]	−16.2 (30%) [0.04][b]	−4.1 (8%)

delocalization within its aromatic ring. Indeed, the benzene ring loses its aromaticity as witnessed by the C–C bond distances elongation to an average value of 1.42 Å compared to that of the free ligand of 1.398 Å and corroborated by its HOMA (Harmonic Oscillator Model of Aromaticity) [94, 95] value of 0.82 conducting to a decreased aromaticity.

It is worth to mention that the interaction energies have been corrected from basis set superposition error (BSSE) with the counterpoise (CP) method developed by Boys and Bernardi [96]. The ΔE_{int} (without BSSE correction) and ΔE^{CP} (with BSSE correction) are given in Tables 1 and 2. The BSSE introduces a nonphysical attraction between the two interacting fragments. Thus, the counterpoise correction usually leads to intermolecular complexes less stable [97]. For all complexes treated in this study, the ΔE_{int} is slightly lower in energies than ΔE^{CP}, where the difference between them do not exceed 1.0 and 2.3 kcal/mol for XCuL' and $[LCuL']^+$, respectively, indicating a negligible influence on interactions, so, in this case, the CP should weakly or even negligibly correct the optimized geometries as well as the interaction energies. It becomes visible from Tables 1 and 2 that the ΔE^{CP} energies arising from total interaction between fragments with BSSE correction obey the same order than that found for ΔE_{int} ones without BSSE correction (Fig. 5).

One of the best characteristics of EDA-NOCV is to decomposing the total orbital interactions (ΔE_{orb}) into pairwise interactions providing the strength and each type of orbital, where the total σ and π orbital contributions into the covalent bonding are gathered in Tables 1 and 2.

For CH_3Cu, the σ-bonding energy towards the L' ligands change drastically from C_2H_2, C_2H_4, and C_4H_6 to C_6H_6 and more to NHC, i.e., they are comparable for C_2H_2, C_2H_4, and C_4H_6, but they enhance for C_6H_6 and more for NHC. We can specify that the proportion of σ and π orbital energies give a higher σ contribution into the ΔE_{orb} component than that of π one, particularly for C_6H_6 and more for NHC ligands.

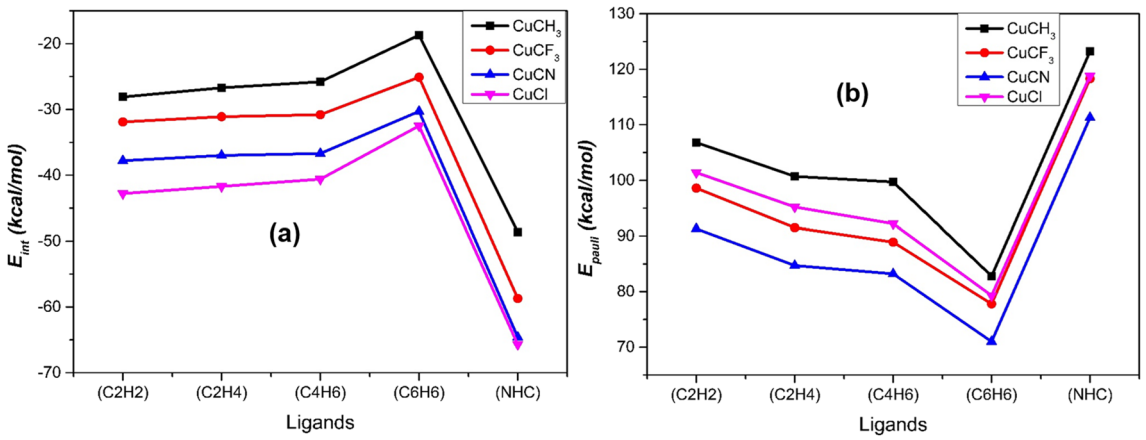

Fig. 4 **a**, **b** ΔE_{int} energy (in kcal/mol) evolution for XCuL' (X = Cl, CN, CH_3, CF_3, and L' = C_2H_2, C_2H_4, C_4H_6, C_6H_6, NHC) compounds obtained by interactions between each XCu and the five L' ligands

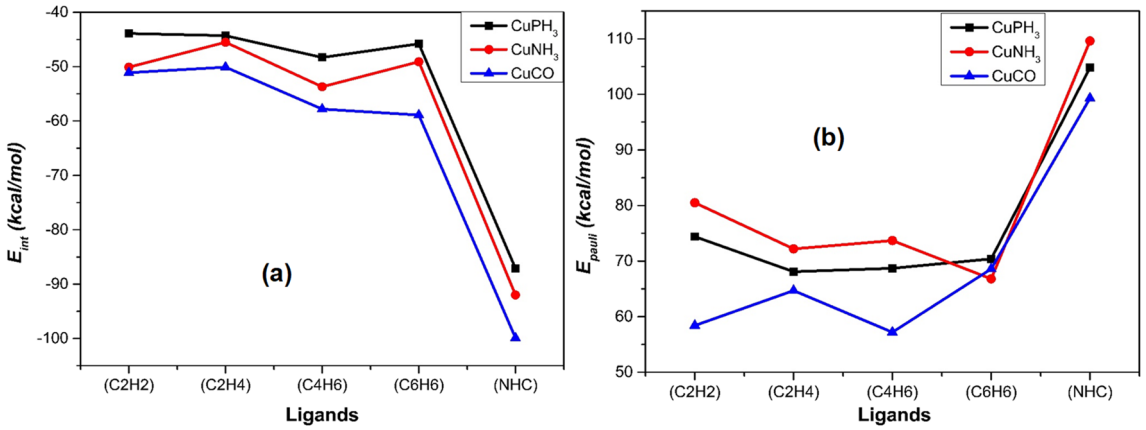

Fig. 5 **a**, **b** ΔE_{int} energy (in kcal/mol) evolution for $(LCuL')^+$ (L = CO, NH_3, PH_3, and L' = C_2H_2, C_2H_4, C_4H_6, C_6H_6, NHC) compounds obtained by interactions between $(LCu)^+$ and the five L' ligands

The ΔE_{orb} component is comparable in both XCuL' and $(LCuL')^+$ compound types, but the absolute values of ΔE_{Pauli} and ΔE_{elstat} are larger in the former species than in the latter, despite the fact that the ΔE_{int} are less significant in XCuL' than in $(LCuL')^+$ due to the difference of natural charges of the interacting fragments in each case. Table 2 shows that the positive charge (NPA) on Cu(I) in the PH_3 complexes has lower values in presence of NHC traducing the strong σ-donation into the vacant metallic orbital. This agrees with the energy decomposition of the orbital interaction term (Table 2), demonstrating that the former species have a higher $\Delta E(\pi)$ contribution than the latter molecules. The EDA analysis of the Cu-C(L') bonding in the presence of CF_3 and CH_3 demonstrates disproportional contributions from electrostatic and covalent interactions and contributions to the latter are less than those to the former. The Cu-L' bonds of the PH_3 and CH_3 ligands have less covalent character and a significant lower degree of π bonding in CF_3 that in CH_3, where a same tendency has been observed for organometallic complexes coordinated in η^2-fashion to L' ligand (L' = C_2H_2, C_2H_4) [98] and related alkyne copper(I) complexes [99].

For ample details regarding the σ-donation and π-backdonation, Tables 1 and 2 gather their amounts obtained for the interacting fragments in XCuL' and $(LCuL')^+$ complexes.

The values given in Fig. 6 highlight electron transfer between the frontier orbitals of the interacting fragments namely CNCu (left side) and NHC (right side), which give information about σ-donation and π-backdonation of the involved orbitals demonstrating a strong σ interaction between 18a orbital of NHC and 12a orbital of CNCu metallic fragment emphasizing a considerable donation of 0.49e of the former and the population by 0.48e of the latter,

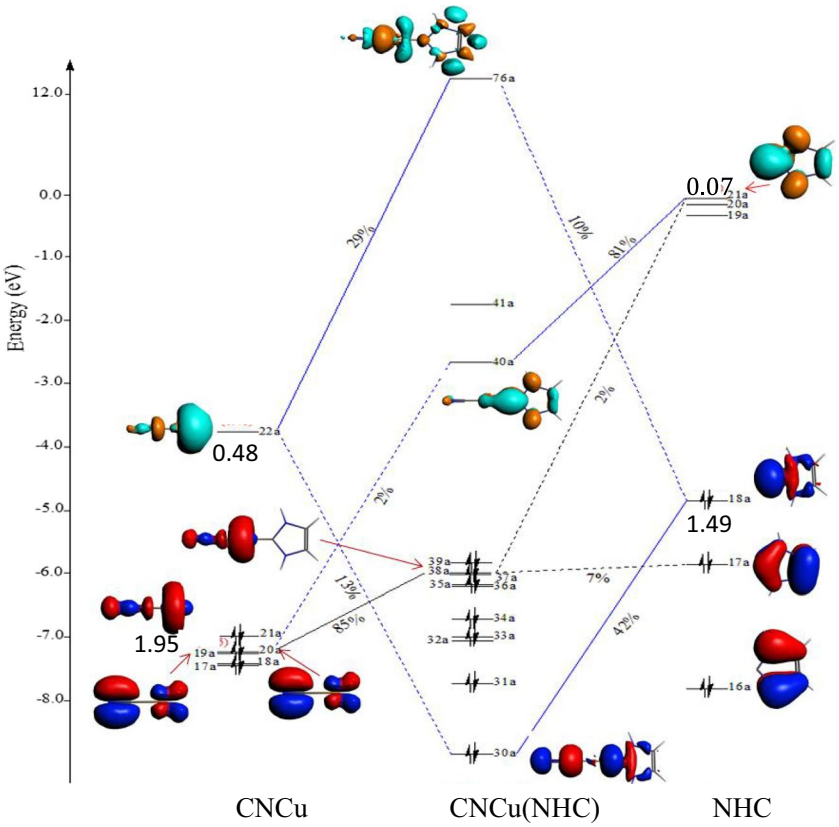

Fig. 6 MO diagram obtained by interactions between CNCu and (NHC) fragments with their frontier orbital populations

while the π-backdonation is weakly stressed between the 19a orbital and 21a one by an electron transfer of 0.07e as described in previous works for related NHC ligands [77].

One can see, that for each XCu or LCu^+ metallic fragment, only one high-lying orbital is involved in the interactions with the L' ligand composed ofd_{z^2}, $d_{x^2-y^2}$, and d_{xy}. As example, for the CNCu(NHC) compound, only the 19a orbital of the CNCu metallic fragment composed of $d_{x^2-y^2}$ (55%) and p_y(19%) of Cu(I) cation that interacted due to its orientation towards the 21a orbital of the NHC ligand, which acquires 0.07e. Similarly, one low-lying vacant σ* antibonding orbital composed mainly of the s orbital of Cu(I) received electron through a σ-donation. At the right side, the NHC ligand presents one high-lying 18a occupied orbital of σ-type composed of s (33%) P_x (32%) and p_y (19%) carbon atomic orbitals which interacted strongly with the 22a metallic fragment orbital composed of a mixing of s (45%), p_x (23%), and p_y (14%) Cu(I) orbitals, beside one antibonding low lying π* orbital. The NHC ligand can be considered Fisher carbene [100] coordinated to a singlet transition metal via a dative carbene to metal σ-donation and a dative metal to carbene π-backdonation.

The breakdown of ΔE_{orb} into pairwise interactions for CNCuL' (L' = C_2H_2, C_2H_4, C_4H_6, C_4H_6, and NHC) complexes is taken as example, which gives rise principally to two orbital contributions ΔE(σ) and ΔE(π) (Table 1) that can be pinpointed by combining deformation densities Δρ(σ) and Δρ(π), respectively, and their associated MOs (Fig. 7). For CNCu(NHC), the NOCV contributions to the deformation density clearly show that the σ-component corresponds to the donation from the lone electron pair of carbon as carbene center towards the *sp*-hydrid orbital of Cu(I) cation as illustrated in Fig. 7e (Top), corresponding to a strong orbital stabilization energy of − 20.5 kcal/mol. While the π-backdonation is due to the electron transfer from the metallic fragment into the empty π* orbital of NHC exhibiting carbon 2p character, it was revealed to be relatively weak with an orbital stabilization energy of − 8.7 kcal/mol. This π-backdonation is weakened by the presence of π^*_{CN} receiving a part of the π-backdonation as described in previous work for related complexes [8]. Accordingly, the orbital interactions are governed by the σ-bonding representing 60% as a contribution into the total orbital interaction. These results are nicely comparable to those obtained by Frenking [83] for the complexes $(CO)_5Cr=CHR$ (R = H, CH_3, CH = CH_2, Ph, C≡CH).

The interaction diagram for CNCu(C_2H_2) displayed in the left side (a) of Fig. S1(a) shows the involvement of the same orbitals of the CNCu fragment encountered in the case of the CNCu(NHC) compound, but with different contributions. Indeed, the C_2H_2 ligand acts as σ-donor through only one orbital of π-type, which is considerably depopulated

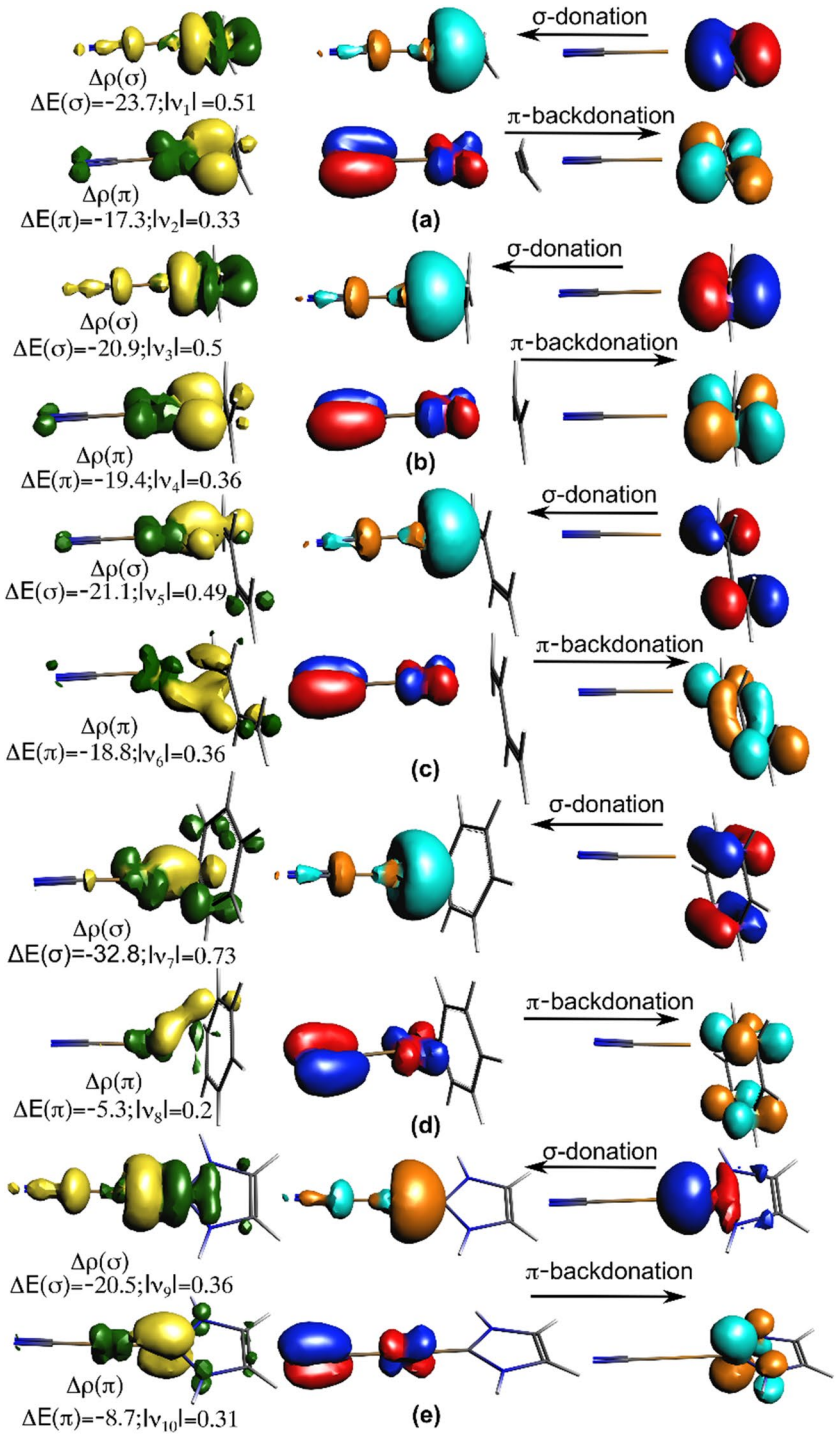

Fig. 7 The contour of the deformation densities Δρ(σ) and Δρ(π) that correspond respectively to ΔE(σ) and ΔE(π) of the complexes $CNCu(C_2H_2)$ (**a**), $CNCu(C_2H_4)$ (**b**), $CNCu(C_4H_6)$ (**c**), $CNCu(C_6H_6)$ (**d**), and CNCu(NHC) (**e**) and their corresponding NOCV orbitals in their singlet state. Isosurface values are 0.0015 au for Δρ(σ) and Δρ(π). The eigenvalues $|\nu_n|$ give the size of the charge migration in electron. The direction of the charge flow of the deformation densities is green → yellow

from 2e to 1.67e in favor of the *sp*-hybrid orbital of CNCu unit receiving 0.38e. This NOCV pairwise contributes to the deformation density Δρ(σ) through an orbital stabilization energy ΔE(σ) of − 23.7 kcal/mol (the top of Fig. 7a). Nevertheless, the π-backdonation is assumed by one high-lying filled *d*-type orbital of CNCu fragment (20a) towards the empty 8a π* orbital reaching an occupation of 0.17e corresponding to one NOCV couple giving rise to an orbital stabilization energy of − 17.3 kcal/mol (the bottom of Fig. 7a).

The MOs diagram given in the right side (b) of Fig. S1(b) matches up to the $CNCu(C_2H_4)$ one showing the interactions between the CNCu and C_2H_4 fragments, stressing clearly the involvement of one orbital of the C_2H_4 fragment namely 8a that undertakes significant occupation decreasing from 2e to 1.69e as illustrated in the left side of Fig. S1(b), through

σ-donation towards the vacant *sp*-hybrid 22a orbital of the CNCu metallic fragment receiving 0.41e as illustrated in the (right side of Fig. S1(b)); thus, this NOCV pairwise contribute into the total ΔE_{orb} by − 21.1 kcal/mol as a stabilization energy ΔE(σ) (the top of Fig. 7b). Inversely, the low-lying π* antibonding 9a orbital of C_2H_4 is involved as an acceptor orbital interacting with the donor 20a orbital of CNCu. This NOCV couple is responsible of the π-backdonation via a stabilization energy of − 18.8 kcal/mol as shown in Fig. 7c (bottom). As can be seen for Table 1, these values show comparable molecular orbital populations for both C_2H_2 and C_2H_4.

Finally, for the CNCu(C_6H_6) compound, the interaction diagram (b) of Fig. S2(b) records the weakest σ-donation from the 21a orbital of the C_6H_6 fragment acting as σ-donor towards the 22a orbital of CNCu fragment which acquires an occupation of 0.43e. Also, the π-backdonation from the 20a orbital of the CNCu moiety into the 22a vacant π* orbital of C_6H_6 is the weakest one compared to those obtained for C_2H_2, C_2H_4, and C_4H_6 ligands, in accordance with energy of − 5.3 kcal/mol, which contributes weakly in the deformation density Δρ(π) as sketched in Fig. 7d (bottom).

However, the NHC ligand turned out to be strong σ-donor, but weak π-acceptor as given in Tables 1 and 2. For the NHC ligand, the NOCV contributions to the deformation density clearly (Fig. 7e) show that the σ-component corresponds to the donation from the lone electron pair of carbon as carbene center, enhanced further by an electron transfer from ancillary halogen atoms. The π-bonding is due to the backdonation from the metal into the empty orbital of X, mostly exhibiting chlorine 3p character in accordance with Cl-Cu-L' bent angle.

It is habitually assumed that the σ bonding contribution for the d.[10] metal ethylene and acetylene complexes prevails over the π-backdonation contribution as observed in previous work [101]

Consequently, the L' → metal σ-donation is twice larger than the metal → L' π-backdonation for L' = C_2H_2, C_2H, and C_4H_6, and it is five or six times larger when L' = C_6H_6 and NHC.

Natural bond orbital analysis

The charge transfer contribution of an NBO pair into the total interaction energy is estimated by the second-order perturbative energy correction [102, 103]. The results collected in Table S3 give emphasis to LP → σ*, σ → LP*, LP → LP*, and σ → σ* donor–acceptor charge transfers occurred between different entities composing the XCuL' and $LCuL'^{+}$ (X = CH_3, Cl, CN, L = NH_3, L' = C_2H_2, C_2H_4, C_4H_6, C_4H_6, and NHC) complexes (σ and σ * correspond to bonding and antibonding orbitals, respectively, and LP and LP* designate lone pair and vacant nonbonding NBOs, respectively). The occupancies of LP and σ designate their population after electron transfers towards the LP* and σ* empty NBOs, while the occupancies of LP* and σ* denote the fractional number of electron transferred from donor to acceptor.

Generally, we observe that LP → σ *, σ → σ*, σ → LP*, and LP → LP* donor–acceptor charge transfers vary from one complex to another and do not obey a specific rule. Indeed, it is noted that the maximum energies corresponding to LP → σ* donor–acceptor giving rise to stabilizing energies between the Cu(I) and the interacting ligands, namely L', X, or L. The donor–acceptor charge transfers are numerous and important in relationship with the magnitudes of the second-order perturbative energies (E^2); for this reason, the values under 10 kcal/mol are not considered. Firstly, the number, the types and the magnitude of the charge transfer of NBO pairs are comparable for CH_3CuL' (L' = C_2H_2, C_2H_4, and C_4H_6), where the second-order perturbative energies (E^2) are in the range 10.6–28.7 kcal/mol matching well with weak or moderate depopulation of one Cu lone pair (LP) from 2e to 1.83e towards C(1)-C(2) σ * NBO which acquires a population of 0.16e. On the other hand, the C(1)-C(2) σ NBO undergoes a depopulation from 2e to 1.84e transferring 0.12e to the vacant Cu (LP*) NBO. It is worth noticing comparable results for $CH_3Cu(C_2H_4)$ and $CH_3Cu(C_4H_6)$ as gathered in Table S3. However, the number of these types of charge transfers is higher in $CH_3Cu(C_6H_6)$, in accordance with the presence of six C–C delocalized bonds, but with comparable values of energies. Secondly, as clearly observed from Table S3, the second-order perturbative energies (E^2) enhance in the presence of NH_3 or NHC as illustrated by the charge transfers namely N(1) → N(1)-C(1) (70.8 kcal/mol) in NH_3Cu(NHC), N → Cu (74.8 kcal/mol) and C(1)-C(2) → Cu (76.8 kcal/mol) in $NH_3Cu(C_6H_6)$, N → Cu (87.3 kcal/mol) and C(1)-C(2) → Cu (95.6 kcal/mol) in $NH_3Cu(C_2H_2)$, N → Cu (78.3 kcal/mol) and C(1)-C(2) → Cu (81.0 kcal/mol) in $NH_3Cu(C_2H_4)$, N → Cu (82.8 kcal/mol) and C(1)-C(2) → Cu (89.7 kcal/mol) in NH_3Cu(C4H6), N(1) → C(2)-C(3) (99.0 kcal/mol) in ClCu(NHC), N(1) → C(2)-C(3) (67.9 kcal/mol) in CNCu(NHC), N(1) → N(1)-C(1) (66.7) in CH_3Cu(NHC), and C(7) → Cu (215.7 kcal/mol) in CNCu(NHC). The second-order perturbative energies (E^2) values show their dependence on the number of the nitrogen atoms involved in the interactions. The strength and the weakness of charge transfers are related to the gain or the loss of electron between the donor and the acceptor moieties. Consequently, based on the stabilization second-order perturbative energies (E^2) are large for NHC and substantially decrease for those of alkenes and alkynes as L' ligands in the presence of CH_3 as X ligand and also increase in the presence of NH_3 as L ligand and in the presence of CN and Cl as X ligands. The second-order perturbative energies (E^2) and the charge densities Increase the charge transfers regardless

the L' ligand amounts the decreasing order of the charge transfers for different complexes is given as follows: Consequently, based on the second-order perturbative energies (E^2) amounts, the decreasing order of the charge transfers for different complexes is given as follows: $ClCu(C_6H_6) \approx CNCu(C_6H_6) > [NH_3Cu(C_2H_2)]^+ \approx [NH_3Cu(C_2H_4)]^+ \approx [NH_3Cu(C_4H_6)]^+ \approx [NH_3Cu(C_6H_6)]^+ > [NH_3Cu(NHC)]^+ \approx CH_3Cu(NHC) > ClCu(NHC) > CNCu(NHC) > ClCu(C_2H_2) \approx ClCu(C_2H_4) \approx ClCu(C_4H_6) > CH_3Cu(C_6H_6) > CNCu(C_2H_2) \approx CNCu(C_2H_4) \approx CNCu(C_4H_6) > CH_3Cu(C_2H_2) \approx CH_3Cu(C_2H_4) \approx CH_3Cu(C_4H_6)$. Therefore, the highest values correspond to the $ClCu(C_6H_6)$, $CNCu(C_6H_6)$, $[NH_3Cu(C_2H_2)]^+$, and $[NH_3Cu(C_2H_4)]^+$ complexes, while the weakest ones are for $CH_3Cu(C_2H_2)$, $CH_3Cu(C_2H_4)$, and $CH_3Cu(C_4H_6)$ complexes.

Conclusion

DFT calculations of the optimized structures and energy decomposition analysis of XCuL' and $(LCuL')^+$ complexes were employed to provide a relationship between the bond lengths, the X-Cu-L' and L-Cu-L' bond angles, the Wiberg indices, Mayer bond orders, bonding energies, and the Cu-L' bonding character. The Mayer bond order offers an appropriate and computationally competent tool of summing *all* the contributions to the bond, giving rise to a bond order around 1, except for the (C_6H_6) ligand, in agreement with the Cu-C bond distances. The energy decomposition analysis indicates that the interactions that occurred for various L' ligands are more electrostatically than covalently bonded to the Cu(I) center, particularly in the presence of C_6H_6 and NHC ligands. The ΔE_{prep} energies highlight weak or negligible deformation of the interacting fragments. Also, ΔE^{CP} corrected energies show a weak impact of the BSSE on the ΔE_{int} energies. The ΔE_{elstst} electrostatic contribution for all η^2-coordination complexes is found slightly around 55 to 60% of the total attractive interaction energy $\Delta E_{elstst} + \Delta E_{orb}$ is more important than that of the orbital one, while this contribution enhances to an average percentage of 75% for all η^1-C(NHC) complexes. The Cu-C bonds of the XCuL' and $(LCuL')^+$complexes are nearly two-thirds ionic and one-third covalent character, except for C_6H_6 and NHC ligands exhibiting more ionic character. The σ-bonding contributes more than 50% into the total orbital interaction overtaking those of π type resulting from σ and π electron transfers. The EDA method gives rise to a coherent scheme of the nature of the chemical bonding, while its extension to the EDA-NOCV offers a link between molecular orbital diagrams and pairwise orbital interactions contributing.

The σ-donation from the filled $\pi_{C\text{-}C}$ bonding orbital to the vacant sp(Cu) acceptor orbital is larger than back-donation from filled metal *d*-orbitals to the $\pi^*_{C\text{–}C}$ or $\pi^*_{C\text{-}N}$.

It is worth noting that the enhancement of π-backbonding reinforces the L-M-L' bending leading to the increased of steric repulsion, which is reduced in the presence of CO and CN^- ligands. Besides, the Cu-NHC π-backbonding is enhanced in presence of chlorine substituent.

The more linear X-Cu-L' and $(L\text{-}Cu\text{-}L')^+$ angles are obtained in the presence of NHC ligand independently on the L or X ligand. Consequently, the ionic character is more pronounced for the XCuL' compounds than that described for the $(LCuL')^+$ ones. Based on the NPA, the Cu oxidation state is comprised between 0 and +I (average $d^{10}s^{0/+1}$ configuration), highlighting the strength of the σ- and π-type interactions, particularly in the NHC cases.

Supplementary Information The online version contains supplementary material available at https://doi.org/10.1007/s11224-024-02366-6.

Acknowledgements The authors are grateful to the Algerian MESRS (ministère de l'Enseignement Supérieur et de la Recherche Scientifique) and the Algerian DGRSDT (Direction Générale de la Recherche Scientifique et du Développement Technologique) for the financial support.

Author contribution Aimen Nadjet: DFT investigation, analysis of the results and writing. Abdallah Zaiter: writing original draft and commented on the final version of the manuscript. Hacene Nemdili: Contributed to study conception and design. Bachir Zouchoune: Conceptualization, manuscript writing and validation. All authors read and approved the final version of the manuscript.

Data availability No datasets were generated or analysed during the current study.

Declarations

Conflict of interest The authors declare no competing interests.

References

1. Gimeno MC, Laguna A (1997) Three- and four-coordinate gold(I) complexes. Chem Rev 97:511–522. https://doi.org/10.1021/cr960361q
2. Vogt J, Mez-Starck B, Vogt N, Hutter W (1999) mogadoc a database for gasphase molecular spectroscopy and structure. J Mol Struct 485–486:249–254. https://doi.org/10.1016/S0022-2860(99)00046-0
3. Harris H, Fisher K, Dance I (2001) Coordination and dehydrogenation of PH $_3$ by 23 transition metal ions in the gas phase: FTICR experiments and density functional interpretations. Inorg Chem 40:6972–6982. https://doi.org/10.1021/ic0105821
4. Schwerdtfeger P, Hermann HL, Schmidbaur H (2003) Stability of the gold(I)−phosphine bond. A comparison with other group 11 elements. Inorg Chem 42:1334–1342. https://doi.org/10.1021/ic026098v
5. Wallesh M, Volz D, Flechon C, Zink DM, Brase S, Baumann T (2014) Organic light emitting material and devices XVIII, ed. F. So, Proc. Of SPIE, 9183, paper 918309.
6. Yesin H, Raush AF, Czerwieniec R, Hofbeck T, Fischer T (2011) The triplet state of organo-transition metal compounds. Triplet harvesting and singlet harvesting for efficient OLEDs. Coord Chem Rev 255:2622–2652

7. Carvajal MA, Novoa JJ, Alvarez S (2004) Choice of coordination number in d ^{10} Complexes of Group 11 Metals. J Am Chem Soc 126:1465–1477. https://doi.org/10.1021/ja038416a
8. Phillips NA, Kong RY, White AJP, Crimmin MR (2021) Group 11 borataalkene complexes: models for alkene activation. Angew Chem Int Ed 60:12013–12019. https://doi.org/10.1002/anie.202100919
9. Sorrell TN, Jameson DL (1983) Synthesis, structure, and reactivity of monomeric two-coordinate copper(I) complexes. J Am Chem Soc 105:6013–6018. https://doi.org/10.1021/ja00357a009
10. Sanyal I, Karlin KD, Strange RW, Blackburn NJ (1993) Chemistry and structural studies on the dioxygen-binding copper-1,2-dimethylimidazole system. J Am Chem Soc 115:11259–11270. https://doi.org/10.1021/ja00077a027
11. Le Clainche L, Giorgi M, Reinaud O (2000) Synthesis and characterization of a novel calix[4]arene-based two-coordinate copper(I) complex that is unusually resistant to dioxygen. Eur J Inorg Chem 2000:1931–1933. https://doi.org/10.1002/1099-0682(200009)2000:9%3c1931::AID-EJIC1931%3e3.0.CO;2-H
12. Liang H-C, Kim E, Incarvito CD, Rheingold AL, Karlin KD (2002) A bis-acetonitrile two-coordinate copper(I) complex: synthesis and characterization of highly soluble $B(C_6F_5)_4^-$ Salts of $[Cu(MeCN)_2]^+$ and $[Cu(MeCN)_4]^+$. Inorg Chem 41:2209–2212. https://doi.org/10.1021/ic010816g
13. Banthia S, Samanta A (2004) In situ reduction of copper(II) forming an unusually air stable linear complex of copper(I) with a fluorescent tag. Inorg Chem 43:6890–6892. https://doi.org/10.1021/ic0490019
14. Zhang Y, Schulz M, Wächtler M, Karnahl M, Dietzek B (2018) Heteroleptic diimine–diphosphine Cu(I) complexes as an alternative towards noble-metal based photosensitizers: design strategies, photophysical properties and perspective applications. Coord Chem Rev 356:127–146. https://doi.org/10.1016/j.ccr.2017.10.016
15. Czerwieniec R, Leitl MJ, Homeier HHH, Yersin H (2016) Cu(I) complexes – thermally activated delayed fluorescence. Photophysical approach and material design. Coord Chem Rev 325:2–28. https://doi.org/10.1016/j.ccr.2016.06.016
16. Föller J, Kleinschmidt M, Marian CM (2016) Phosphorescence or thermally activated delayed fluorescence? Intersystem crossing and radiative rate constants of a three-coordinate copper(I) complex determined by quantum-chemical methods. Inorg Chem 55:7508–7516. https://doi.org/10.1021/acs.inorgchem.6b00818
17. Hamze R, Peltier JL, Sylvinson D, Jung M, Cardenas J, Haiges R, Soleilhavoup M, Jazzar R, Djurovich PI, Bertrand G, Thompson ME (2019) Eliminating nonradiative decay in Cu(I) emitters: >99% quantum efficiency and microsecond lifetime. Science 363:601–606. https://doi.org/10.1126/science.aav2865
18. Di D, Romanov AS, Yang L, Richter JM, Rivett JPH, Jones S, Thomas TH, Abdi Jalebi M, Friend RH, Linnolahti M, Bochmann M, Credgington D (2017) High-performance light-emitting diodes based on carbene-metal-amides. Science 356:159–163. https://doi.org/10.1126/science.aah4345
19. Hamze R, Jazzar R, Soleilhavoup M, Djurovich PI, Bertrand G, Thompson ME (2017) Phosphorescent 2-, 3- and 4-coordinate cyclic (alkyl)(amino)carbene (CAAC) Cu(I) complexes. Chem Commun 53:9008–9011. https://doi.org/10.1039/C7CC02638B
20. Li J, Wang L, Zhao Z, Li X, Yu X, Huo P, Jin Q, Liu Z, Bian Z, Huang C (2020) Two-coordinate copper(I)/NHC complexes: dual emission properties and ultralong room-temperature phosphorescence. Angew Chem Int Ed 59:8210–8217. https://doi.org/10.1002/anie.201916379
21. Cao L, Huang S, Liu W, Zhao H, Xiong XG, Zhang JP, Fu LM, Yan X (2020) Thermally activated delayed fluorescence from d^{10}-metal carbene complexes through intermolecular charge transfer and multicolor emission with a monomer–dimer equilibrium. Chem Eur J 26:17222–17229. https://doi.org/10.1002/chem.202004106
22. Romanov AS, Di D, Yang L, Fernandez-Cestau J, Becker CR, James CE, Zhu B, Linnolahti M, Credgington D, Manfred B (2016) Highly photoluminescent copper carbene complexes based on prompt rather than delayed fluorescence. Chem Commun 52:6379–6382. https://doi.org/10.1039/C6CC02349E
23. Gernert M, Meller U, Haehnel M, Pflaum J, Steffen AA (2017) Cyclic alkyl(amino)carbene as two-atom -chromophore leading to the first phosphorescent linear CuI complexes. Chem Eur J 23:2206–2216
24. Lee M, Nguyen M, Brandt C, Gleiter R, Zsolnai L, Driess A, Huttner G, Lang H (2017) Catalytic hydroalkylation of allenes. Angew Chem Int Ed 56:15703–15707. https://doi.org/10.1002/anie.201709144
25. Wang G, Pecher L, Frenking G, Dias HVR (2018) Vinyltrifluoroborate complexes of silver supported by *N*-heterocyclic carbenes. Eur J Inorg Chem 2018:4142–4152. https://doi.org/10.1002/ejic.201800899
26. Daniela BD, Fausto C, Robert D, Straehle J, Weiss H (1987) Olefin complexes of gold(I) by carbonyl displacement from carbonylgold(I) chloride. Organometallics 6:1207–1210. https://doi.org/10.1021/om00149a014
27. Davila RM, Staples RJ, Fackler JPJr (1994) Synthesis and structural characterization of Au4(MNT)(dppee)2(Cl)2. cntdot.1/4CH2Cl2 (MNT = 1,2-dicyanoethene-1,2-dithiolate-S, S'; dppee = cis-Bis(diphenylphosphino)ethylene): a Gold(I) metal-olefin complex in which the olefin orientation relative to the coordination plane involving the metal is defined. Organometallics 13:418–420. https://doi.org/10.1021/om00014a007
28. Mingos DMP, Yau J, Menzer S, Williams DJ (1995) A gold(I) [2]catene. Angew Chem Int Ed Engl 34:1894–1895. https://doi.org/10.1002/anie.199518941
29. Lang H, Köhler K, Zsolnai L (1996) Unusual coordination mode of organogold(I) compounds: trigonal-planar complexation of gold (I) centers by alkynes. Chem Commun 2043–2044. https://doi.org/10.1039/CC9960002043
30. Köhler K, Silverio SJ, Hyla-Kryspin I (1997) Trigonal-planar-coordinated organogold(I) complexes stabilized by organometallic 1,4-diynes: reaction behavior, structure, and bonding. Organometallics 16:4970–4979. https://doi.org/10.1021/om970302i
31. Schulte P, Behrens U (1998) Strong coordination of cycloheptynes by gold(i) chloride: synthesis and structure of two complexes of the type [(alkyne)AuCl]. Chem Commun 1633–1634. https://doi.org/10.1039/a803791d.
32. Otsuka S, Yoshida T, Matsumoto M, Nakatsu K (1976) Bis(tertiary phosphine)palladium(0) and -platinum(0) complexes: preparations and crystal and molecular structures. J Am Chem Soc 98:5850–5858. https://doi.org/10.1021/ja00435a017
33. Dinjus E, Leitner W (1995) New insights into the palladium-catalysed synthesis of δ-lactones from 1,3-dienes and carbon dioxide. Appl Organomet Chem 9:43–50. https://doi.org/10.1002/aoc.590090108
34. Morokuma K (1971) Molecular orbital studies of hydrogen bonds. III. C=O···H–O hydrogen bond in H2CO···H2O and H2CO···2H2O. J Chem Phys 55:1236–1244. https://doi.org/10.1063/1.1676210
35. Ziegler T, Rauk A (1979) Carbon monoxide, carbon monosulfide, molecular nitrogen, phosphorus trifluoride, and methyl isocyanide as sigma. donors and pi acceptors. A theoretical study by the Hartree-Fock-Slater transition-state method. Inorg Chem 18:1755–1759. https://doi.org/10.1021/ic50197a006
36. Ziegler T, Rauk A (1979) A theoretical study of the ethylene-metal bond in complexes between copper(1+), silver(1+), gold(1+), platinum(0) or platinum(2+) and ethylene, based on

the Hartree-Fock-Slater transition-state method. Inorg Chem 18:1558–1565. https://doi.org/10.1021/ic50196a034
37. Mitoraj MP, Michalak A, Ziegler T (2009) A combined charge and energy decomposition scheme for bond analysis. J Chem Theory Comput 5:962–975. https://doi.org/10.1021/ct800503d
38. Michalak A, Mitoraj M, Ziegler T (2008) Bond orbitals from chemical valence theory. J Phys Chem A 112:1933–1939. https://doi.org/10.1021/jp075460u
39. Mitoraj M, Michalak A (2007) Natural orbitals for chemical valence as descriptors of chemical bonding in transition metal complexes. J Mol Model 13:347–355. https://doi.org/10.1007/s00894-006-0149-4
40. Mitoraj M, Michalak A (2008) Applications of natural orbitals for chemical valence in a description of bonding in conjugated molecules. J Mol Model 14:681–687. https://doi.org/10.1007/s00894-008-0276-1
41. Mitoraj M, Michalak A (2007) Donor–acceptor properties of ligands from the natural orbitals for chemical valence. Organometallics 26:6576–6580. https://doi.org/10.1021/om700754n
42. Fukui K (1975) Theory of orientation and stereoselection. Springer Verlag, Berlin
43. Woodward RB, Hoffmann R (1970) The Conservation of Orbital Symmetry. Verlag Chemie, Weinheim
44. Becke AD (1986) Density functional calculations of molecular bond energies. J Chem Phys 84:4524–4529. https://doi.org/10.1063/1.450025
45. Becke AD (1988) Density-functional exchange-energy approximation with correct asymptotic behavior. Phys Rev A 38:3098–3100. https://doi.org/10.1103/PhysRevA.38.3098
46. Perdew JP (1986) Density-functional approximation for the correlation energy of the inhomogeneous electron gas. Phys Rev B 33:8822–8824. https://doi.org/10.1103/PhysRevB.33.8822
47. Perdew JP (1986) Erratum: density-functional approximation for the correlation energy of the inhomogeneous electron gas. Phys Rev B 34:7406–7406. https://doi.org/10.1103/PhysRevB.34.7406
48. Becke A (1993) Density-functional thermochemistry III The role of exact exchange. J Chem Phys 98:5648
49. Lee C, Yang W, Parr RG (1988) Development of the Colle-Salvetti correlation-energy formula into a functional of the electron density. Phys Rev B 37:785–789. https://doi.org/10.1103/PhysRevB.37.785
50. Vosko SD, Wilk L, Nusair M (1980) Accurate, spin-dependent electron liquid correlation energies for local spin density calculations: a critical analysis. Can J Chem 58:1200–1211. https://doi.org/10.1139/p80-159
51. ADF2022.01. SCM, Theoretical chemistry, Vrije Univ. Amsterdam. Nethlands. http://www.scm.com.
52. Baerends EJ, Ellis DE, Ros P (1973) Self-consistent molecular Hartree—Fock—Slater calculations I. The computational procedure Chem Phys 2:41–51. https://doi.org/10.1016/0301-0104(73)80059-X
53. Te Velde G, Baerends EJ (1992) Numerical integration for polyatomic systems. J Comput Phys 99:84–98. https://doi.org/10.1016/0021-9991(92)90277-6
54. Fonseca Guerra C, Snijders JG, Te Velde G, Baerends EJ (1998) Towards an order- N DFT method. Theor Chem Acc Theory Comput Model Theor Chim Acta 99:391–403. https://doi.org/10.1007/s002140050353
55. Bickelhaupt FM, Baerends EJ (2000) Kohn-Sham density functional theory: predicting and understanding chemistry. In: Lipkowitz KB, Boyd DB (eds) Reviews in Computational Chemistry, 1st edn. Wiley, pp 1–86
56. Te Velde G, Bickelhaupt FM, Baerends EJ, Fonseca Guerra C, van Gisbergen SJA, Ziegler T (2001) Chemistry with ADF. J Comput Chem 22:931–967. https://doi.org/10.1002/jcc.1056
57. Fan L, Ziegler T (1992) Application of density functional theory to infrared absorption intensity calculations on main group molecules. J Chem Phys 96:9005–9012. https://doi.org/10.1063/1.462258
58. Fan L, Ziegler T (1992) Application of density functional theory to infrared absorption intensity calculations on transition-metal carbonyls. J Phys Chem 96:6937–6941. https://doi.org/10.1021/j100196a016
59. Wiberg KB (1968) Application of the pople-santry-segal CNDO method to the cyclopropylcarbinyl and cyclobutyl cation and to bicyclobutane. Tetrahedron 24:1083–1096. https://doi.org/10.1016/0040-4020(68)88057-3
60. Weinhold F, Landis CR (2005) Valency and bonding: a natural bond orbital donor-acceptor perspective. Cambridge University Press
61. Glendening ED, Badenhoop JK, Reed AE, Carpenter JE, Bohmann J, A, Morales CM, Karafilogou P, Landis CR, Weinhold F (2021) NBO 7.0, Theoretical Chemistry Institute, University of Wisconsin, Madison. In: Nat. Bond Orbital Homepage. https://nbo7.chem.wisc.edu/.
62. Mayer I (1983) Charge, bond order and valence in the AB initio SCF theory. Chem Phys Lett 97:270–274. https://doi.org/10.1016/0009-2614(83)80005-0
63. Mayer I (1984) Bond order and valence: relations to Mulliken's population analysis. Int J of Quantum Chemistry 26:151–154. https://doi.org/10.1002/qua.560260111
64. Bridgeman AJ, Cavigliasso G, Ireland LR (2001) Rothery J (2001) The Mayer bond order as a tool in inorganic chemistry. J Chem Soc Dalton Trans 14:2095–2108. https://doi.org/10.1039/b102094n
65. Herzberg G Molecular spectra and molecular structure: III. Electronic spectra and electronic structure of polyatomic molecules. Ed., Van Nostrand, New York, 1966, Vol 3.
66. Craig NC, Oertel CM, Oertel DC, Tubergen MJ, Lavrich RJ, Chaka AM (2002) Structure of *cis, trans* -1,4-difluorobutadiene from microwave spectroscopy. J Phys Chem A 106:4230–4235. https://doi.org/10.1021/jp014378a
67. Craig NC, Groner P, McKean DC (2006) Equilibrium structures for butadiene and ethylene: compelling evidence for Π-electron delocalization in butadiene. J Phys Chem A 110:7461–7469. https://doi.org/10.1021/jp060695b
68. Durig JR (2000) Equilibrium structural parameters, 1st edn. Elsevier, Amsterdam, New York
69. Zendaoui S-M, Zouchoune B (2016) Coordination chemistry of mixed M(benzene)(cyclopendadienyl) sandwich complexes: electronic properties and bonding analysis. New J Chem 40:2554–2564. https://doi.org/10.1039/C5NJ02595H
70. Naili N, Zouchoune B (2018) Structural diversity of homobinuclear transition metal complexes of the phenazine ligand: theoretical investigation. Struct Chem 29:725–739. https://doi.org/10.1007/s11224-017-1064-2
71. Nemdili H, Zouchoune B, Saber Zendaoui M, Ferhati A (2019) Structural, bonding and redox properties of 34-electron bimetallic complexes and their oxidized 32- and 33-electron and reduced 35- and 36-electron derivatives containing the indenyl fused π-system: A DFT overview. Polyhedron 160:219–228. https://doi.org/10.1016/j.poly.2018.12.049
72. Farah S, Ababsa S, Benhamada N, Zouchoune B (2010) Theoretical investigation of the coordination of dibenzazepine to

transition-metal complexes: a DFT study. Polyhedron 29:2722–2730. https://doi.org/10.1016/j.poly.2010.06.020
73. Bouchakri N, Benmachiche A, Zouchoune B (2011) Bonding analysis and electronic structure of transition metal–benzoquinoline complexes: a theoretical study. Polyhedron 30:2644–2653. https://doi.org/10.1016/j.poly.2011.07.012
74. Mansouri L, Zouchoune B (2015) Substitution effects and electronic properties of the azo dye (1-phenylazo-2-naphthol) species: a TD-DFT electronic spectra investigation. Can J Chem 93:509–517. https://doi.org/10.1139/cjc-2014-0436
75. Zouchoune B, Mansouri L (2019) Electronic structure and UV–Vis spectra simulation of square planar Bis(1-(4-methylphenylazo)-2-naphtol)-transition metal complexes [M(L)2]x (M = Ni, Pd, Pt, Cu, Ag, and x = − 1, 0, + 1): DFT and TD-DFT study. Struct Chem 30:691–701. https://doi.org/10.1007/s11224-018-1215-0
76. Benmachiche A, Zendaoui S, Bouaoud S, Zouchoune B (2013) Electronic structure and coordination chemistry of phenanthridine ligand in first-row transition metal complexes: a DFT study. Int J Quantum Chem 113:985–996. https://doi.org/10.1002/qua.24071
77. Mokrane Z, Zouchoune B, Zaiter A (2020) Coordination's preference and electronic structure of N-heterocyclic carbene–monometallic complexes: DFT evaluation of σ-bonding and π-backbonding interactions. Theor Chem Acc 139:114. https://doi.org/10.1007/s00214-020-02628-6
78. Raubenheimer HG, Cronje S, Olivier PJ (1995) Synthesis and characterization of mono(carbene) complexes of copper and crystal structure of a linear thiazolinylidene compound. J Chem Soc Dalton Trans 313. https://doi.org/10.1039/dt9950000313.
79. Belyakov AV, Altova EP, Rykov AN, Sharanov PY, Shishkov IF, Romanov AS (2023) The equilibrium molecular structure of cyclic (alkyl)(amino) carbene copper (I) chloride via gas-phase electron diffraction and quantum chemical calculations. Molecules 28:6897
80. Lewis GN. Valence and the structure of atoms and molecules. Chemical Catalog Company, Incorporated 1923.
81. Wolters LP, Bickelhaupt FM (2013) Nonlinear d^{10}-ML_2 transition-metal complexes. ChemistryOpen 2:106–114. https://doi.org/10.1002/open.201300009
82. Khireche M, Zouchoune B, Ferhati A, Nemdili H, Zerizer MA (2021) Understanding the chemical bonding in sandwich complexes of transition metals coordinated to nine-membered rings: energy decomposition analysis and the donor–acceptor charge transfers. Theor Chem Acc 140:122. https://doi.org/10.1007/s00214-021-02802-4
83. Frenking G, Fröhlich N (2000) The nature of the bonding in transition-metal compounds. Chem Rev 100:717–774. https://doi.org/10.1021/cr980401l
84. Frenking G, Wichmann K, Fröhlich N, Grobe J, Le Van D, Krebs B, Golla W, Läge M (2002) Nature of the metal−ligand bond in $M(CO)_5PX_3$ complexes (M = Cr, Mo, W; X = H, Me, F, Cl): synthesis, molecular structure, and quantum-chemical calculations. Organometallics 21:2921–2930. https://doi.org/10.1021/om020311d
85. Zaiter A, Zouchoune B (2018) Electronic structure and energy decomposition of binuclear transition metal complexes containing β-diketiminate and imido ligands: spin state and metal's nature effects. Struct Chem 29:1307–1320. https://doi.org/10.1007/s11224-018-1112-6
86. Zerizer MA, Nemdili H, Zouchoune B (2022) Electron transfers' assessment between stannol ring of triple-decker complexes and M(CO)5 (M = Cr, Mo, W), MnCp(CO)2 and CoCp(CO) metallic fragments: bonding and energy decomposition analysis. Polyhedron 223:115960. https://doi.org/10.1016/j.poly.2022.115960
87. Mecheri S, Zouchoune B, Zendaoui S-M (2020) Bonding and electronic structures in dinuclear (X)[(Ind)M2L2] complexes (M = Ni, Pd, L = CO, PEt3, X = Cl, Allyl, Ind = indenyl, Cp = cyclopentadienyl): analogy between four-electron donor ligands. Theor Chem Acc 139:12. https://doi.org/10.1007/s00214-019-2526-y
88. Mecheri S, Zouchoune B (2023) Terminal and bridging ligand effects on M(I)-M(I) multiple bonding: a DFT investigation of the coordination in (X)[M 2 Cl] L 2 complexes (M = Cr, Fe, L = CO, PEt 3, X = Cl, allyl, Cp, and indenyl). Int J Quantum Chem 123:e27089. https://doi.org/10.1002/qua.27089
89. Mecheri S, Zouchoune B (2023) Donor-acceptor electron transfers and bonding performance of cyclopentadienyl and cyclo-P5 middle decks in (CpFeE5)ML3 and (CpFeE5)FeCb (E5 = Cp, P5 and ML3 = Cr(CO)3, Mo(CO)3, CrBz, MnCp, MoBz) triple-decker complexes: bonding and energy decomposition analysis. Polyhedron 244:116586. https://doi.org/10.1016/j.poly.2023.116586
90. Benaïssa A, Bouhadiba A, Naili N, Chekkal F, Khelfaoui M, Bouras I, Madjram MS, Zouchoune B, Mogali S, Malfi N, Nouar L, Madi F (2023) Computational investigation of dimethoate and β-cyclodextrin inclusion complex: molecular structures, intermolecular interactions, and electronic analysis. Struct Chem 34:1189–1204. https://doi.org/10.1007/s11224-023-02162-8
91. Naili N, Kahlal S, Zouchoune B, Saillard JY, Braunstein P (2023) Carbonylmetallates as versatile 2-, 4- or 6-electron donor metalloligands in transition-metal complexes and clusters: a global approach. Chem Eur J 29:e202203557. https://doi.org/10.1002/chem.202203557
92. Hafsi Y, Mecheri S, Zouchoune B (2023) Molecular and electronic structures, bonding analysis, and UV–Vis spectra predictions of quinolino[3,2-b]benzodiazepine and quinolino[3,2-b]benzoxazepine metal transition M(L)2Cl2 and M(L)Cl2 complexes. Struct Chem 34:2051–2064. https://doi.org/10.1007/s11224-023-02145-9
93. Zhao L, von Hopffgarten M, Andrada DM, Frenking G (2017) Energy decomposition analysis. WIREs Comput Mol Sci e1345. https://doi.org/10.1002/wcms.1345.
94. Kruszewski J, Krygowski TM (1972) Definition of aromaticity basing on the harmonic oscillator model. Tetrahedron Lett 13:3839–3842. https://doi.org/10.1016/S0040-4039(01)94175-9
95. Krygowski TM, Szatylowicz H, Stasyuk OA, Dominikowska J, Palusiak M (2014) aromaticity from the viewpoint of molecular geometry: application to planar systems. Chem Rev 114:6383–6422. https://doi.org/10.1021/cr400252h
96. Boys SF, Bernardi F (1970) The calculation of small molecular interactions by the differences of separate total energies. Some procedures with reduced errors. Mol Phys 19:553–566. https://doi.org/10.1080/00268977000101561
97. Zouchoune B (2020) How the ascorbic acid and hesperidin do improve the biological activities of the cinnamon: theoretical investigation. Struct Chem 31:2333–2340. https://doi.org/10.1007/s11224-020-01594-w
98. Massera C, Frenking G (2003) Energy partitioning analysis of the bonding in L2TM-C2H2 and L2TM-C2H4 (TM = Ni, Pd, Pt; L2 = PH3)2, (PMe3)2, H2PCH2PH2, H2P(CH2)2PH2). Organometallics 22:2758–2765

99. Noonikara-Poyil A, Muñoz-Castro A, Rasika Dias HV (2022) Terminal and internal alkyne complexes and azide-alkyne cycloaddition chemistry of copper(I) supported by a fluorinated bis(pyrazolyl)borate. Molecules 27:16–31. https://doi.org/10.3390/molecules27010016
100. Taylor TE, Hall MB (1984) Theoretical comparison between nucleophilic and electrophilic transition metal carbenes using generalized molecular orbital and configuration interaction methods. J Am Chem Soc 106:1576–1584. https://doi.org/10.1021/ja00318a007
101. Mehara J, Watson BT, Noonikara-Poyil A, Zacharias AO, Roithová J, Rasika Dias HV (2022) Binding interactions in copper, silver and gold π-complexes. Chemistry 28:e202103984. https://doi.org/10.1002/chem.202103984]
102. Reed AE, Curtiss LA, Weinhold FA (1988) Intermolecular interactions from a natural bond orbital, donor-acceptor viewpoint. Chem Rev 88:899–926
103. Weinhold FA (1997) Nature of H-bonding in clusters, liquids, and enzymes: an ab initio, natural bond orbital perspective. J Mol Struct 398:181–197